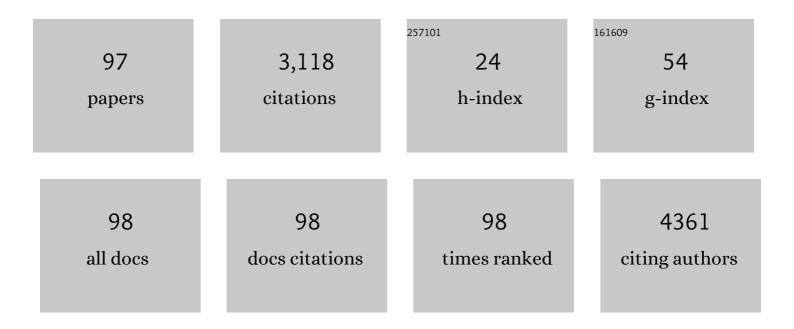
## Hieu T Nguyen

List of Publications by Year in descending order

Source: https://exaly.com/author-pdf/7978988/publications.pdf Version: 2024-02-01



HIELL T NOUVEN

#	Article	IF	CITATIONS
1	All-perovskite tandem solar cells with 24.2% certified efficiency and area over 1 cm2 using surface-anchoring zwitterionic antioxidant. Nature Energy, 2020, 5, 870-880.	19.8	497
2	Interface passivation using ultrathin polymer–fullerene films for high-efficiency perovskite solar cells with negligible hysteresis. Energy and Environmental Science, 2017, 10, 1792-1800.	15.6	381
3	Uncertainty analysis for the coefficient of band-to-band absorption of crystalline silicon. AIP Advances, 2015, 5, .	0.6	313
4	Nanoscale localized contacts for high fill factors in polymer-passivated perovskite solar cells. Science, 2021, 371, 390-395.	6.0	270
5	Structural engineering using rubidium iodide as a dopant under excess lead iodide conditions for high efficiency and stable perovskites. Nano Energy, 2016, 30, 330-340.	8.2	133
6	Light and Electrically Induced Phase Segregation and Its Impact on the Stability of Quadruple Cation High Bandgap Perovskite Solar Cells. ACS Applied Materials & Interfaces, 2017, 9, 26859-26866.	4.0	114
7	Origin of Efficiency and Stability Enhancement in Highâ€Performing Mixed Dimensional 2Dâ€3D Perovskite Solar Cells: A Review. Advanced Functional Materials, 2022, 32, 2009164.	7.8	96
8	Temperature dependence of the band-band absorption coefficient in crystalline silicon from photoluminescence. Journal of Applied Physics, 2014, 115, .	1.1	80
9	Efficient and Layerâ€Dependent Exciton Pumping across Atomically Thin Organic–Inorganic Typeâ€I Heterostructures. Advanced Materials, 2018, 30, e1803986.	11.1	79
10	Ultralow Absorption Coefficient and Temperature Dependence of Radiative Recombination of CH <sub>3</sub> NH <sub>3</sub> PbI <sub>3</sub> Perovskite from Photoluminescence. Journal of Physical Chemistry Letters, 2015, 6, 767-772.	2.1	73
11	Temperature dependence of the radiative recombination coefficient in crystalline silicon from spectral photoluminescence. Applied Physics Letters, 2014, 104, .	1.5	58
12	Mechanisms and Applications of Steady-State Photoluminescence Spectroscopy in Two-Dimensional Transition-Metal Dichalcogenides. ACS Nano, 2020, 14, 14579-14604.	7.3	56
13	Understanding the Role of Vanadium Vacancies in BiVO <sub>4</sub> for Efficient Photoelectrochemical Water Oxidation. Chemistry of Materials, 2021, 33, 3553-3565.	3.2	54
14	Hydrogenation of Phosphorus-Doped Polycrystalline Silicon Films for Passivating Contact Solar Cells. ACS Applied Materials & Interfaces, 2019, 11, 5554-5560.	4.0	47
15	Combined Bulk and Surface Passivation in Dimensionally Engineered 2Dâ€3D Perovskite Films via Chlorine Diffusion. Advanced Functional Materials, 2021, 31, 2104251.	7.8	37
16	Quantifying Quasiâ€Fermi Level Splitting and Mapping its Heterogeneity in Atomically Thin Transition Metal Dichalcogenides. Advanced Materials, 2019, 31, e1900522.	11.1	34
17	In Situ Formation of Mixedâ€Dimensional Surface Passivation Layers in Perovskite Solar Cells with Dualâ€Isomer Alkylammonium Cations. Small, 2020, 16, e2005022.	5.2	34
18	Modulated interlayer charge transfer dynamics in a monolayer TMD/metal junction. Nanoscale, 2019, 11, 418-425.	2.8	33

#	Article	IF	CITATIONS
19	Multiwavelength Single Nanowire InGaAs/InP Quantum Well Light-Emitting Diodes. Nano Letters, 2019, 19, 3821-3829.	4.5	32
20	Supertransport of excitons in atomically thin organic semiconductors at the 2D quantum limit. Light: Science and Applications, 2020, 9, 116.	7.7	32
21	Micrometer-Scale Deep-Level Spectral Photoluminescence From Dislocations in Multicrystalline Silicon. IEEE Journal of Photovoltaics, 2015, 5, 799-804.	1.5	29
22	Microâ€photoluminescence spectroscopy on heavilyâ€doped layers of silicon solar cells. Physica Status Solidi - Rapid Research Letters, 2015, 9, 230-235.	1.2	28
23	Dislocations in laser-doped silicon detected by micro-photoluminescence spectroscopy. Applied Physics Letters, 2015, 107, .	1.5	27
24	Radial Growth Evolution of InGaAs/InP Multi-Quantum-Well Nanowires Grown by Selective-Area Metal Organic Vapor-Phase Epitaxy. ACS Nano, 2018, 12, 10374-10382.	7.3	26
25	Influence of PECVD deposition temperature on phosphorus doped poly-silicon passivating contacts. Solar Energy Materials and Solar Cells, 2020, 206, 110348.	3.0	24
26	Light-activated inorganic CsPbBr <sub>2</sub> I perovskite for room-temperature self-powered chemical sensing. Physical Chemistry Chemical Physics, 2019, 21, 24187-24193.	1.3	23
27	Emission Control from Transition Metal Dichalcogenide Monolayers by Aggregation-Induced Molecular Rotors. ACS Nano, 2020, 14, 7444-7453.	7.3	23
28	Twist-driven wide freedom of indirect interlayer exciton emission in MoS2/WS2 heterobilayers. Cell Reports Physical Science, 2021, 2, 100509.	2.8	23
29	Highly Enhanced Light–Matter Interaction in MXene Quantum Dots–Monolayer WS <sub>2</sub> Heterostructure. Small, 2021, 17, e2006309.	5.2	22
30	Complementary bulk and surface passivations for highly efficient perovskite solar cells by gas quenching. Cell Reports Physical Science, 2021, 2, 100511.	2.8	21
31	Characterizing amorphous silicon, silicon nitride, and diffused layers in crystalline siliconsolarcellsusingmicro-photoluminescence spectroscopy. Solar Energy Materials and Solar Cells, 2016, 145, 403-411.	3.0	18
32	Sub-Bandgap Luminescence from Doped Polycrystalline and Amorphous Silicon Films and Its Application to Understanding Passivating-Contact Solar Cells. ACS Applied Energy Materials, 2018, 1, 6619-6625.	2.5	18
33	Imaging Spatial Variations of Optical Bandgaps in Perovskite Solar Cells. Advanced Energy Materials, 2019, 9, 1802790.	10.2	18
34	Deposition pressure dependent structural and optoelectronic properties of ex-situ boron-doped poly-Si/SiOx passivating contacts based on sputtered silicon. Solar Energy Materials and Solar Cells, 2020, 215, 110602.	3.0	17
35	Microscopic Distributions of Defect Luminescence From Subgrain Boundaries in Multicrystalline Silicon Wafers. IEEE Journal of Photovoltaics, 2017, 7, 772-780.	1.5	16
36	Morphology, microstructure, and doping behaviour: A comparison between different deposition methods for poly‧i/SiO <sub><i>x</i></sub> passivating contacts. Progress in Photovoltaics: Research and Applications, 2021, 29, 857-868.	4.4	16

#	Article	IF	CITATIONS
37	Impact of Carrier Profile and Rear-Side Reflection on Photoluminescence Spectra in Planar Crystalline Silicon Wafers at Different Temperatures. IEEE Journal of Photovoltaics, 2015, 5, 77-81.	1.5	15
38	Ring defects in n-type Czochralski-grown silicon: A high spatial resolution study using Fourier-transform infrared spectroscopy, micro-photoluminescence, and micro-Raman. Journal of Applied Physics, 2018, 124, 243101.	1.1	14
39	Hydrogenation Mechanisms of Polyâ€&i/SiO <sub><i>x</i></sub> Passivating Contacts by Different Capping Layers. Solar Rrl, 2020, 4, 1900476.	3.1	13
40	Growth of Oxygen Precipitates and Dislocations in Czochralski Silicon. IEEE Journal of Photovoltaics, 2017, 7, 735-740.	1.5	12
41	Dynamically Gasâ€Phase Switchable Super(de)wetting States by Reversible Amphiphilic Functionalization: A Powerful Approach for Smart Fluid Gating Membranes. Advanced Functional Materials, 2018, 28, 1704423.	7.8	12
42	Aluminium and zinc co-doped CuInS2 QDs for enhanced trion modulation in monolayer WS2 toward improved electrical properties. Journal of Materials Chemistry C, 2019, 7, 15074-15081.	2.7	12
43	Hydrogen-Assisted Defect Engineering of Doped Poly-Si Films for Passivating Contact Solar Cells. ACS Applied Energy Materials, 2019, 2, 8783-8791.	2.5	12
44	On the composition of luminescence spectra from heavily doped p-type silicon under low and high excitation. Journal of Luminescence, 2017, 181, 223-229.	1.5	11
45	All room-temperature synthesis, N2 photofixation and reactivation over 2D cobalt oxides. Applied Catalysis B: Environmental, 2022, 304, 121001.	10.8	11
46	Optical Evaluation of Silicon Wafers With Rounded Rear Pyramids. IEEE Journal of Photovoltaics, 2017, 7, 1596-1602.	1.5	10
47	Hydrogenation Mechanisms of Poly‣i/SiO <sub><i>x</i></sub> Passivating Contacts by Different Capping Layers. Solar Rrl, 2020, 4, 2070033.	3.1	10
48	Comparison of firing stability between p―and nâ€ŧype polysilicon passivating contacts. Progress in Photovoltaics: Research and Applications, 2022, 30, 970-980.	4.4	10
49	Quantifying boron and phosphorous dopant concentrations in silicon from photoluminescence spectroscopy at 79 K. Physica Status Solidi (A) Applications and Materials Science, 2016, 213, 3029-3032.	0.8	9
50	Spatially and Spectrally Resolved Absorptivity: New Approach for Degradation Studies in Perovskite and Perovskite/Silicon Tandem Solar Cells. Advanced Energy Materials, 2020, 10, 1902901.	10.2	9
51	Boron Spin-On Doping for Poly-Si/SiO <sub><i>x</i></sub> Passivating Contacts. ACS Applied Energy Materials, 2021, 4, 4993-4999.	2.5	9
52	Low-temperature micro-photoluminescence spectroscopy on laser-doped silicon with different surface conditions. Applied Physics A: Materials Science and Processing, 2016, 122, 1.	1.1	8
53	Effects of Solar Cell Processing Steps on Dislocation Luminescence in Multicrystalline Silicon. Energy Procedia, 2015, 77, 619-625.	1.8	7
54	Determination of Dopant Density Profiles of Heavily Boron-Doped Silicon From Low Temperature Microphotoluminescence Spectroscopy. IEEE Journal of Photovoltaics, 2017, 7, 1693-1700.	1.5	7

#	Article	IF	CITATIONS
55	Hydrogenation in multicrystalline silicon: The impact of dielectric film properties and firing conditions. Progress in Photovoltaics: Research and Applications, 2020, 28, 493-502.	4.4	7
56	Contactless and Spatially Resolved Determination of Currentâ^'Voltage Curves in Perovskite Solar Cells via Photoluminescence. Solar Rrl, 2021, 5, 2100348.	3.1	7
57	Electrical properties of perovskite solar cells by illumination intensity and temperatureâ€dependent photoluminescence imaging. Progress in Photovoltaics: Research and Applications, 2022, 30, 1038-1044.	4.4	7
58	Photoluminescence Excitation Spectroscopy of Diffused Layers on Crystalline Silicon Wafers. IEEE Journal of Photovoltaics, 2016, 6, 746-753.	1.5	6
59	Detecting Dopant Diffusion Enhancement at Grain Boundaries in Multicrystalline Silicon Wafers With Microphotoluminescence Spectroscopy. IEEE Journal of Photovoltaics, 2017, 7, 598-603.	1.5	6
60	Photoluminescence Spectra of Moderately Doped, Compensated Silicon Si:P,B at 79–300 K. IEEE Journal of Photovoltaics, 2017, 7, 581-589.	1.5	6
61	Activation Kinetics of the Boron–oxygen Defect in Compensated n- and p-type Silicon Studied by High-Injection Micro-Photoluminescence. IEEE Journal of Photovoltaics, 2017, 7, 988-995.	1.5	6
62	Quantification of Sheet Resistance in Boronâ€Diffused Silicon Using Microâ€Photoluminescence Spectroscopy at Room Temperature. Solar Rrl, 2017, 1, 1700088.	3.1	6
63	Precipitation of Cu and Ni in n- and p-type Czochralski-grown silicon characterized by photoluminescence imaging. Journal of Crystal Growth, 2017, 460, 98-104.	0.7	5
64	Perovskite Solar Cells: Imaging Spatial Variations of Optical Bandgaps in Perovskite Solar Cells (Adv.) Tj ETQq0 0	0 rgBT /O 10.2	verlock 10 Tf
65	Efficient Passivation and Low Resistivity for p <sup>+</sup> -Si/TiO <sub>2</sub> Contact by Atomic Layer Deposition. ACS Applied Energy Materials, 2020, 3, 6291-6301.	2.5	5
66	Firing Stability of Polysilicon Passivating Contacts: The Role of Hydrogen. , 2021, , .		5
67	Zero-emission multivalorization of light alcohols with self-separable pure H2 fuel. Applied Catalysis B: Environmental, 2021, 292, 120212.	10.8	5
68	Tuning the crystal structure and optical properties of selective area grown InGaAs nanowires. Nano Research, 2022, 15, 3695-3703.	5.8	5
69	Effective Passivation of InGaAs Nanowires for Telecommunication Wavelength Optoelectronics. Advanced Optical Materials, 2022, 10, .	3.6	5
70	Experimental Determination of the Uncertainty of the Absorption Coefficient of Crystalline Silicon. Energy Procedia, 2015, 77, 170-178.	1.8	4
71	Reconstructing photoluminescence spectra at liquid nitrogen temperature from heavily boronâ€doped regions of crystalline silicon solar cells. Progress in Photovoltaics: Research and Applications, 2018, 26, 587-596.	4.4	4
72	Imaging the Thickness of Passivation Layers for Crystalline Silicon with Micronâ€Scale Spatial Resolution Using Spectral Photoluminescence. Solar Rrl, 2017, 1, 1700157.	3.1	3

#	Article	IF	CITATIONS
73	Characterization of Epitaxial Heavily Doped Silicon Regions Formed by Hot-Wire Chemical Vapor Deposition Using Micro-Raman and Microphotoluminescence Spectroscopy. IEEE Journal of Photovoltaics, 2018, 8, 813-819.	1.5	3
74	Investigation of Gallium–Boron Spinâ€On Codoping for poly‣i/SiO <sub><i>x</i></sub> Passivating Contacts. Solar Rrl, 2021, 5, 2100653.	3.1	3
75	Evaluating Depth Distributions of Dislocations in Silicon Wafers Using Micro-Photoluminescence Excitation Spectroscopy. Energy Procedia, 2016, 92, 145-152.	1.8	2
76	Contactless, nondestructive determination of dopant profiles of localized boron-diffused regions in silicon wafers at room temperature. Scientific Reports, 2019, 9, 10423.	1.6	2
77	Solar Cells: Quantifying Quasiâ€Fermi Level Splitting and Mapping its Heterogeneity in Atomically Thin Transition Metal Dichalcogenides (Adv. Mater. 25/2019). Advanced Materials, 2019, 31, 1970180.	11.1	2
78	Hydrogenation of polycrystalline silicon films for passivating contacts solar cells. , 2019, , .		2
79	A Correlative Study of Film Lifetime, Hydrogen Content, and Surface Passivation Quality of Amorphous Silicon Films on Silicon Wafers. IEEE Journal of Photovoltaics, 2020, 10, 1307-1312.	1.5	2
80	Micro-photoluminescence studies of shallow boron diffusions below polysilicon passivating contacts. Solar Energy Materials and Solar Cells, 2021, 227, 111108.	3.0	2
81	Impact of Gettering and Hydrogenation on Sub-Band-Gap Luminescence from Ring Defects in Czochralski-Grown Silicon. ACS Applied Energy Materials, 2021, 4, 11258-11267.	2.5	2
82	Interfacing transition metal dichalcogenides with chromium germanium telluride quantum dots for controllable light-matter interactions. Journal of Colloid and Interface Science, 2022, 611, 432-440.	5.0	2
83	Characterization of Cu and Ni Precipitates in n– and p-type Czochralski-grown Silicon by Photoluminescence. Energy Procedia, 2016, 92, 880-885.	1.8	1
84	Micro-photoluminescence studies of shallow phosphorus diffusions below polysilicon passivating contacts. Solar Energy Materials and Solar Cells, 2020, 218, 110780.	3.0	1
85	Imaging pseudo current-voltage characteristics of perovskite solar cells using Suns-photoluminescence. , 2021, , .		1
86	Contactless and Spatially Resolved Determination of Currentâ^'Voltage Curves in Perovskite Solar Cells via Photoluminescence. Solar Rrl, 2021, 5, 2170083.	3.1	1
87	Photoluminescence Spectroscopy of Thermal Donors and Oxygen Precipitates Formed in Czochralski Silicon at 450 ŰC. IEEE Journal of Photovoltaics, 2022, 12, 222-229.	1.5	1
88	Investigation of Gallium–Boron Spinâ€On Codoping for polyâ€5i/SiO <sub><i>x</i></sub> Passivating Contacts. Solar Rrl, 2021, 5, .	3.1	1
89	Silicon Luminescence Spectra Modelling and the Impact of Dopants. Energy Procedia, 2016, 92, 852-856.	1.8	0
90	Modeling Photoluminescence Spectra in Heavily Boron Doped Silicon. , 2018, , .		0

#	Article	IF	CITATIONS
91	Predicting Open-Circuit Voltages in Atomically-Thin Monolayer Transition Metal Dichalcogenides-Based Solar Cells. , 2019, , .		0
92	Luminescence from poly-Si films and its application to study passivating-contact solar cells. , 2019, , .		0
93	Extracting optical bandgaps from luminescence images of perovskite solar cells. , 2019, , .		0
94	Tandem Solar Cells: Spatially and Spectrally Resolved Absorptivity: New Approach for Degradation Studies in Perovskite and Perovskite/Silicon Tandem Solar Cells (Adv. Energy Mater. 4/2020). Advanced Energy Materials, 2020, 10, 2070016.	10.2	0
95	Comparative studies of optoelectronic properties, structures, and surface morphologies for phosphorus-doped poly-Si/SiOx passivating contacts. , 2021, , .		0
96	Mechanisms of luminescence in silicon photovoltaics. , 2021, , .		0
97	Correction to "Boron Spin-On Doping for Poly-Si/SiOx Passivating Contactsâ€: ACS Applied Energy Materials, 2021, 4, 6376-6376.	2.5	0